Received: 30 April 2021 | Revised: 8 June 2021 | Accepted: 9 June 2021 | Published on: 8 July 2021

DOI: 10.1002/ctpp.202100083

ORIGINAL ARTICLE

Contributions to Plasma Physics

Variation of filamentation phenomenon in strongly magnetized plasma with various discharge parameters

Mohamad Menati | **Uwe Konopka** | **Edward Thomas Jr.**

Physics Department, Auburn University, Auburn, Alabama, USA

Correspondence
Mohamad Menati, Physics Department, Auburn University, Auburn, Al, USA, 36849.
Email: mzm0085@auburn.edu

Funding information
Alabama NSF EPSCoR, Grant/Award Number: OIA-1655280; US Department of Energy, Grant/Award Number: SC-0016330

Abstract

Filamentation phenomenon is one of the most important outcomes of applying a strong magnetic field to low-pressure plasmas and dusty plasmas. In this article, the variation of filamentation phenomenon with neutral gas pressure and plasma density will be investigated using numerical simulations. It will be shown through these simulations how the formation of the filamentary patterns in the magnetized plasma results in a localized electric field structure that strongly contributes to the properties of the filamentary patterns. Based on the results of the simulations, a theoretical model is derived that relates the width of the filamentary patterns to the plasma density. The model has been successfully employed to predict the width of the patterns emerging in various simulations of the magnetized plasma.

KEYWORDS

dusty plasma, filamentation, magnetized dusty plasma, magnetized plasma, pattern formation

1 | INTRODUCTION

The presence of charged solid particulate matter in plasmas in the form of "dusty" plasmas has been a vibrant topic of research for over 30 years. The presence of these charged, nanometre to micrometre-sized particles adds to the complexity and richness of the plasma by introducing a fourth component to the system of electrons, ions, and neutral atoms. The large mass and a small charge-to-mass ratio of the dust particles, as compared to the other charged particles in the plasma, enables the emergence of new types of self-organized[1–3] and collective behaviours.[4–7]

Over time, the dusty plasma research community has made significant advances in understanding the coupling between the background plasma and the "dust" particles. In particular, the works of Fortov and co-workers have made important contributions to advancing the understanding of dusty plasmas. Some of the earliest reported studies of both weakly and strongly coupled dusty plasmas in dc glow discharges[8–10] and the very first microgravity studies of dusty plasmas in space[11–14] were led by Fortov and his colleagues. Through both detailed experimental and theoretical investigations, their team has been at the forefront of dusty plasma research.

Fortov and colleagues also made some of the earliest contributions to understanding the role of magnetic fields in the dynamics of dusty plasmas. For example, one of their earliest works was the development of a model for "dusty" molecules in a magnetic field.[15] In later works, their team performed early studies of dust cloud rotation under the influence of magnetic fields in the striations of a dc discharge plasma, which showed the reversal of the rotation direction with increasing magnetic fields in the range of 0–2,500 G.[16–18] While the observed dust rotation is believed to be due to the coupling between the ion $E \times B$ drift and the dust, the reversal of the dust rotation was attributed to the reversal in the radial electrical field that appears as the electrons and ion diffusion become decoupled due to the confinement of the electrons by the magnetic field, which modifies the plasma potential profile.

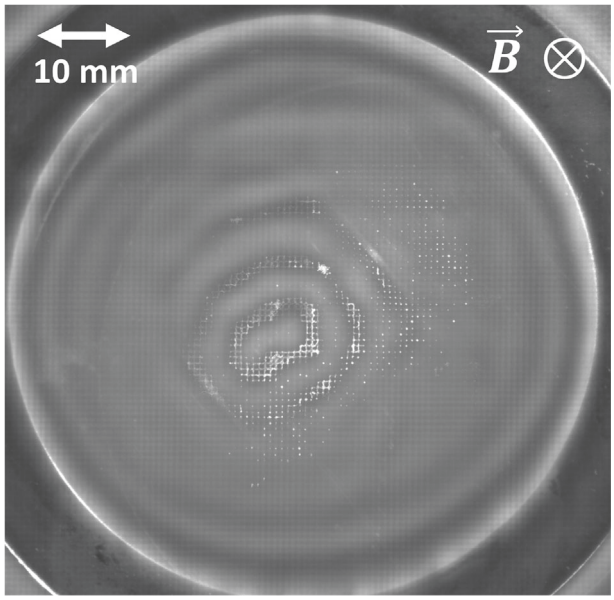

FIGURE 1 Top view of the interior of the Magnetized Dusty Plasma Experiment (MDPX) device at Auburn University. The filamentary structures are visible as the grey spirals. The dust particles are the while dots and lines as a result of summing 500 frames individual video frames 8 μm diameter dust particles suspended in an argon plasma at a pressure, $p = 16.6$ Pa (125 mTorr), a radio frequency (rf) input power, $P_{RF} = 1.6$ W, at 13.56 MHz, and a magnetic field of $B = 2.5$ T. *Source:* Adapted from data set: MAX_20150212_rf1p6_p125_B2p5_12p5fps_022_Vp0.png, Auburn University

These early works on magnetic field effects are among the studies that have motivated our own studies of the influence of magnetic fields on dusty plasmas. In particular, at even higher magnetic fields, $B \geq 5{,}000$ G, it has been shown in several previous works that the plasma itself can produce a wide variety of spatial structures that can directly compete with the dusty plasma phenomena that are of interest. An example of this is shown in Figure 1 from the Magnetized Dusty Plasma Experiment (MDPX) device at Auburn University.[19,20] In Figure 1, a top view of a dust cloud in the MDPX device is shown with the magnetic field pointing into the page. The image sums up 500 frames of 8 μm diameter dust particles suspended in an argon plasma at a pressure, $p = 16.6$ Pa (125 mTorr), a radio frequency (rf) input power, $P_{RF} = 1.6$ W, at 13.56 MHz, and a magnetic field of $B = 2.5$ T. The image reveals the competition between the previously reported dust gridding phenomenon (i.e., the rectangular grid pattern formed by the dust particle motion, shown as white lines in the image)[21–23] and the light grey, spiral structures observed in the visible light glow of the plasma (i.e., filamentary structures).[24–29] Therefore, in order to understand the dynamics of the dust particles in strongly magnetized plasmas, it is essential that we understand the underlying plasma dynamics. This paper is motivated by these observations and focuses on furthering the understanding of this pattern formation in the background plasma at high magnetic fields.

Filamentary patterns are self-organized structures within a strongly magnetized plasma that differ from the rest of plasma in terms of parameters such as density, optical brightness, and electron temperature.[24–29] Formation of these self-organized patterns in low-pressure magnetized plasmas (filamentation phenomenon) has been observed for over two decades.[24–29] These patterns are extended in the discharge along the magnetic axis, channelling from one sheath region to another. So far, filamentation phenomenon has been reported to appear at very low pressure ($P \leq 20$ Pa) plasmas that are exposed to strong magnetic fields ($B \geq 1$ T).

The formation and properties of the filamentary patterns in magnetized plasmas can be affected by various parameters such as neutral gas pressure, magnetic field, type of the discharge gas, electrodes conductivity, and the geometry of the plasma chamber.[25,27,29] Schwabe et al.[25] experimentally investigated the variation of filamentation phenomenon with gas pressure and magnetic field strength and showed the strong dependence of the phenomenon on the ion Hall parameter (the ratio of the ions mean-free-path to their gyro-radius). The effect of the ion Hall parameter along with the impact of electrode conductivity and gas type on filamentation phenomenon was also identified in numerical simulations of the phenomenon by Menati et al.[27,29] Despite all the efforts, introducing a comprehensive theoretical framework that successfully describes the formation mechanism of filamentary structures in strongly magnetized plasmas and their dependency on the aforementioned parameters is still an ongoing research study.

The main challenge to perform precise experimental studies on the filamentation phenomenon is the lack of an established diagnostic method for measurements of plasma parameters in strongly magnetized plasmas.[30,31] In addition to that, due to the complicated nature of the filamentary structures, application of optical measurement methods such as laser induced fluorescence (LIF) is limited.[25–29] Therefore, numerical and theoretical investigation of the magnetized plasma remains one of the most effective ways of studying this phenomenon.

In this article, we will show how the effect of the strong magnetic field on the mobility and diffusion coefficient of the electrons and ions contributes to the formation of filamentary structures in magnetized plasmas. In the presence of strong magnetic field, the cross-field transport of the electrons is extremely suppressed, while the ions can still have a limited transport perpendicular to the magnetic axis, which is a crucial basis for filamentation phenomenon.[32,33] The results of the simulations show that there is a critical dependence of the filamentation phenomenon of three fundamental scale lengths in the plasma: the ion gyro-radius, the ion-neutral mean-free-path, and the electron Debye length. Because these parameters depend upon the neutral gas pressure and the plasma density, the variation of the filamentation as a function of these quantities will be studied in detail. Based on the results of these numerical simulations, a theoretical model will be presented that successfully relates the width of the filaments to the plasma density.

The rest of this article is organized as follows. In Section 2, the results of numerical simulation of filamentation phenomenon under variation of pressure and plasma density will be presented. Section 3 discusses a theoretical approach to the stability of filamentary structures. Finally, Section 4 gives a summary of the work.

2 | NUMERICAL SIMULATION OF FILAMENTATION PHENOMENON

In order to gain an insight into the physical processes that govern the formation of filamentary structures in magnetized plasmas, a series of simulations have been performed under variation of neutral gas pressure (neutral density) and average electron/ion density. Controlling these parameters correspond to particular plasma scale lengths, specifically the electron Debye length, ion-neutral mean-free-path, and ion gyro-radius. This work will show that these length scales (and the ratios of these length scales) may be important in determining the properties of the filaments. Therefore, all simulation results presented in this article are labelled with a set of three length parameters; (r_i (mm), λ_i (mm), λ_{De} (mm)), which represent ion gyro-radius, ion-neutral mean-free-path, and electron Debye length, respectively. In an unmagnetized plasma, these parameters are calculated through the following equations:

$$r_i = \frac{m_i V_{th_i}}{qB} \tag{1}$$

$$\lambda_i = \frac{V_{th_i}}{\nu_i} \tag{2}$$

$$\lambda_{De} = \sqrt{\frac{\varepsilon_0 K_b T_e}{e^2 n_e}} \tag{3}$$

in which m_i is the mass of the ions, V_{th_i} is thermal velocity of the ions, q is the charge of the ions, B is the magnetic field, ν_i is ion-neutral collision frequency, ε_0 is electric permittivity of free space, K_b is the Boltzmann constant, T_e is electron temperature, e is the unit charge, and n_e is the background electron density.

All the simulation results presented in this article are performed in our modelling platform, Rectangular Model for Magnetized Plasma Simulations (REMAPS), which is extensively explained in Reference [29]. In general, the simulations will start with a uniform background plasma (equal density for ions and electrons) within a 6.3 cm × 6.3 cm × 4.2 cm simulation volume. Therefore, for a plasma at a neutral gas pressure of 10 Pa, the simulation volume is about 60 λ_i × 60 λ_i × 40 λ_i. The electrons and ions temperatures are set to $T_e = 2.5$ eV, and $T_i = 0.025$ eV, respectively, and are held constant for the duration of the simulations. Also, all plasma chamber walls are assumed to be grounded and fully absorbent for electrons and ions. The absorption of the ions in fact is a result of an assumed recombining with electrons supported by the chamber walls.

A schematic drawing of the rectangular plasma chamber that is considered in the simulations is depicted in Figure 2.

REMAPS is a 3D fluid model in which the governing equations for the motion of both electrons and ions are taken into account. Since the temperatures of electrons/ions are assumed to be constant in the model, it only solves Poisson's equation along with momentum and continuity for electrons and ions. The full set of equations in REMAPS for individual

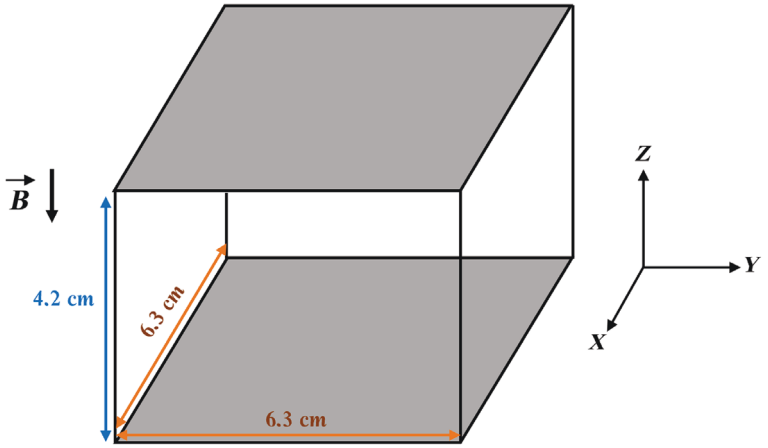

FIGURE 2 Schematic drawing of the rectangular plasma chamber considered in REMAPS for the simulations of filamentary patterns in magnetized plasmas. The picture is not drawn to scale

species α (= e, i—for electrons and ions) is given below:

$$\nabla^2\varphi = \frac{\rho}{\varepsilon} \tag{4}$$

$$q_\alpha n_\alpha(\boldsymbol{E} + \boldsymbol{V}_\alpha \times \boldsymbol{B}) - \boldsymbol{\nabla} P_\alpha - m_\alpha n_\alpha \upsilon_{\alpha-n}\boldsymbol{V}_\alpha = m_\alpha n_\alpha \left(\frac{\partial \boldsymbol{V}_\alpha}{\partial \boldsymbol{t}} + (\boldsymbol{V}_\alpha.\boldsymbol{\nabla})\boldsymbol{V}_\alpha\right) \tag{5}$$

$$\boldsymbol{\Gamma}_{\boldsymbol{\alpha}} = n_\alpha \boldsymbol{V}_{\boldsymbol{\alpha}} \tag{6}$$

$$\frac{\partial n_\alpha}{\partial t} + \nabla \cdot \boldsymbol{\Gamma\alpha} = S - L \tag{7}$$

where ρ is the charge density given by $e(n_\mathrm{i} - n_\mathrm{e})$, and ε is the electric permittivity, q_α is charge, n_α is density, $\boldsymbol{E}$ is electric field vector given by $-\boldsymbol{\nabla\varphi}$, $\boldsymbol{V}_\alpha$ is velocity vector, $\boldsymbol{B}$ is magnetic field vector, P_α is pressure, m_α is mass, $\nu_{\alpha\text{-}n}$ is collision frequency with neutral atoms, $\boldsymbol{\Gamma}_{\boldsymbol{\alpha}}$ is flux vector, S is ionization rate, and L is recombination rate of the electrons and ions.

The loss term L in Equation (7) is just from fluxes reaching the boundaries (walls). We assume that losses from recombination of ions and electrons in the plasma bulk are negligible as the ionization fraction of the system is very low, of order 10^{-7}. In our simulations, we set a target electron density for each simulation run and adjust the source term S accordingly to compensate for any losses to the walls. Therefore, we feed back the lost electrons as electron/ion pairs distributed proportional to the already present local electron density in the plasma volume.

2.1 | Filamentation under variation of neutral gas pressure

In the first set of the simulations, the neutral gas pressure was varied while other plasma parameters are held constant. In these simulations, the electron/ion densities are $n_\mathrm{e} = n_\mathrm{i} = 5.4 \times 10^{15}\,\mathrm{m}^{-3}$, electron temperature was $T_\mathrm{e} = 2.5$ eV, ion temperature $T_\mathrm{i} = 0.025$ eV, and magnetic field was $B = 0.8$ T. The neutral gas pressure was given four different values of 6, 12, 31, and 46 Pa (45, 90, 232, and 345 mTorr). The X-Y cross section (top view) of the electron density profiles at the centre of the plasma chamber for these simulations is displayed in Figure 3. All the simulation results presented in this article are taken from the middle of the plasma chamber at $Z = 2.1$ cm.

The same spatial pattern appears in the ion density and plasma potential profile and therefore they are not shown here. Moreover, the patterns displayed here extend through the discharge along the magnetic field direction. Figure 3 shows that by decreasing the pressure (increasing ion mean-free-path) the pattern formed in the plasma get thinner and therefore a higher number of the filamentary curves fit within the simulated plasma chamber. Also, it is noticed in Figure 3.a that, when the ion mean-free-path gets smaller than the ions gyro-radius at high pressures ($\lambda_\mathrm{i} < r_\mathrm{i}$), filamentary patterns do not form in the plasma. This observation is confirmed in simulations performed using different sets of plasma parameters and has previously seen in other simulations[23,29] and also in the experimental studies of filamentation phenomenon.[25,26,28]

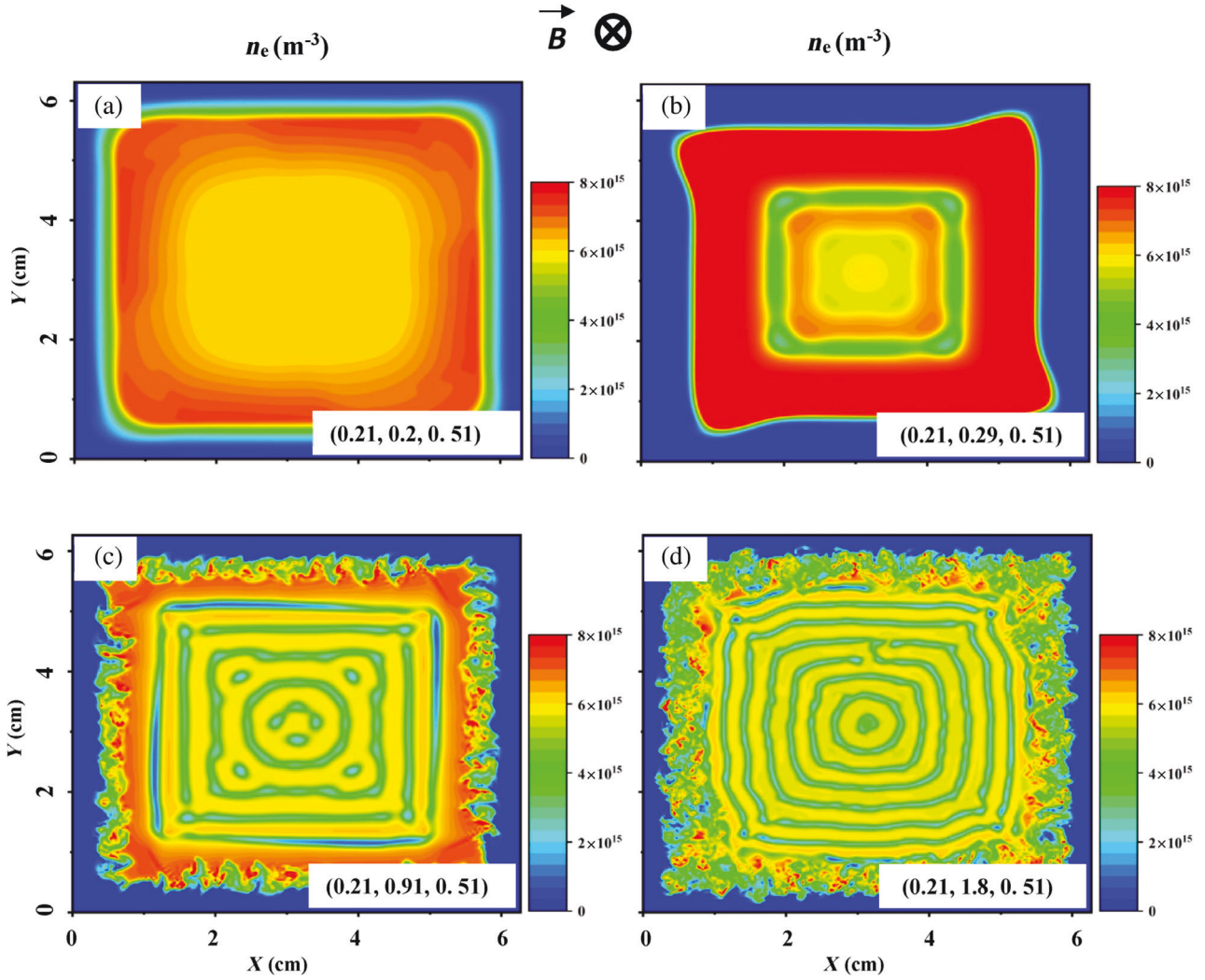

FIGURE 3 X-Y cross section of the electron density profile in magnetized argon plasma at different neutral gas pressure. (a) 46 Pa, (b) 31 Pa, (c) 12 Pa, (d) 6 Pa. The electron/ion densities are 5.4×10^{14} m^{-3}, the plasma is exposed to $B = 0.8$ T magnetic field, while $T_e = 2.5$ eV and $T_i = 0.025$ eV. The set of three length parameters; (r_i (mm), λ_i (mm), λ_{De} (mm)), is also displayed on each graph. By increasing the pressure so that the ion mean-free-path drops below the ion gyro-radius, no significant filamentary pattern forms in the magnetized plasma

To verify the presumption that ion gyro-radius must be smaller than ions mean-free-path in the magnetized plasma to support formation of filamentary structures, the ion gyro-radius (r_i) is reduced to 0.1 mm by increasing the magnetic field from 0.8 T to 1.6 T while keeping all other parameters as the simulation presented in Figure 3a. Figure 4 shows the X-Y cross section of the electron density profile for this case. It is clear from this graph that, by decreasing the ion gyro-radius below the ion mean-free-path, filamentary patterns form again in the plasma. This observation was also tested and confirmed in simulations using different sets of plasma parameters.

The continuous patterns formed in these simulations are rectangular closer to the walls and more curved in the centre of the discharge. This suggests that the rectangular boundary condition assumed in these simulations is imposing its shape to the filamentary patterns. It is noted that in the experiments, a circular ring is usually placed on the electrode, which may be enforcing the observed circular patterns [2, 1, 3]. Moreover, the whole plasma rotates due to the presence of the magnetic field and the background electric field, which has been also observed in the experiments [1, 3]. As a result, in the sheath regions where electric field is strong, this flow of the plasma along the walls presumably Kelvin–Helmholtz instability appears to develop. Our conclusion here is supported by the observation that these instabilities, which cause the roughness of the plasma near the walls, are suppressed at higher pressures due to higher collision rates with neutral gas atoms (see Figure 3b).

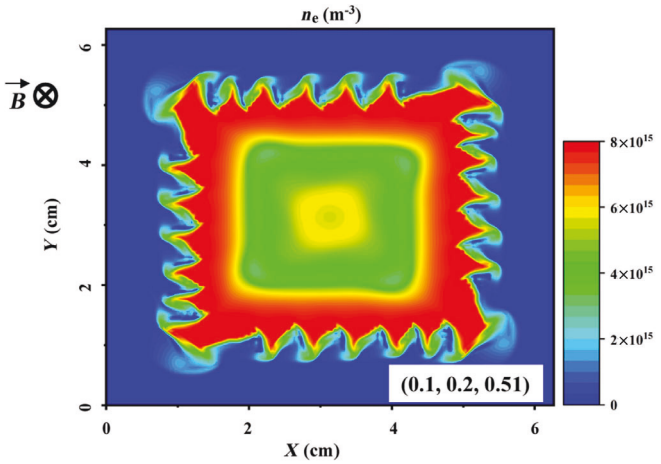

FIGURE 4 X-Y cross section of the electron density profile in argon plasma for $P = 46$ Pa and $n_e = n_i = 5.4 \times 10^{14}$ m^{-3}, $T_e = 2.5$ eV and $T_i = 0.025$ eV, with a background magnetic field of 1.6 T. The set of three length parameters, (r_i (mm), λ_i (mm), λ_{De} (mm)), is also displayed on the graph. This graph compared to Figure 23.a shows the formation of filamentary structures in magnetized plasma when the ion mean-free-path is larger than the ion gyro-radius in the plasma

2.2 | Filamentation under variation of background plasma density

In another set of simulations, the background plasma density was varied while all other parameters were kept constant ($P = 15$ Pa, $B = 0.8$ T, $T_e = 2.5$ eV, and $T_i = 0.025$ eV). Due to the contribution of the electron density to the electron Debye length (Equation 3), this set of simulations is equivalent to changing electron Debye length (or ion Debye length) while keeping other length scales constant. The X-Y cross section (top view) of the electron density profiles at the centre of the plasma chamber for these simulations is displayed in Figure 5.

Figure 5 shows that by increasing the electron Debye length (decreasing the electron/ion densities), the number of filamentary curves in the plasma decreases and the patterns get wider. Also, similar to the role of the ions mean-free-path, if the electron Debye length is less than the ions gyro-radius, no significant pattern forms in the plasma (see Figure 5a). Although variation of input power in the experimental studies of filamentation phenomenon does not necessarily correspond to mere variation of plasma density, the mitigation of filamentation by increasing the RF power in those experiments can be interpreted as a confirmation for this observation.[25,26,28]

To verify this, the ion gyro-radius (r_i) was reduced to 0.1 mm by increasing the magnetic field from 0.8 T to 1.6 T. Figure 6 shows the X-Y cross section of the electron density profile for this case in which a maze-like filamentary structure forms as r_i drops below the Debye length.

3 | THEORETICAL APPROACH TO THE STABILITY OF THE SELF-ORGANIZED STRUCTURES

The above simulation results show that there is a correlation between filamentation and electron scale lengths in the plasma that may be giving us some insights into the behaviour of these strongly magnetized plasmas. This can be seen through a more detailed examination of the electron and ion density and potential profiles that are formed in the simulations. Although the electron and ion density profiles in a magnetized plasma are very similar, the density of the electrons drops more than the ions in the depletion regions (the regions in between filamentary rings where the density of electron/ions has dropped below the background plasma density). This observation is displayed in Figure 7, which represents the variation of electron/ion densities (Figure 7a) as well as the plasma potential (Figure 7b) along x-axis in the middle of the magnetized plasma chamber. Such a plasma potential and the resultant electric field structure are crucial in maintaining the filamentary structures in magnetized plasmas.[23] These density and plasma potential profile suggest a balance between the electric force due to the local electric field and the force resulting from the gradient of density at the boundary of filament/depletion regions.[23]

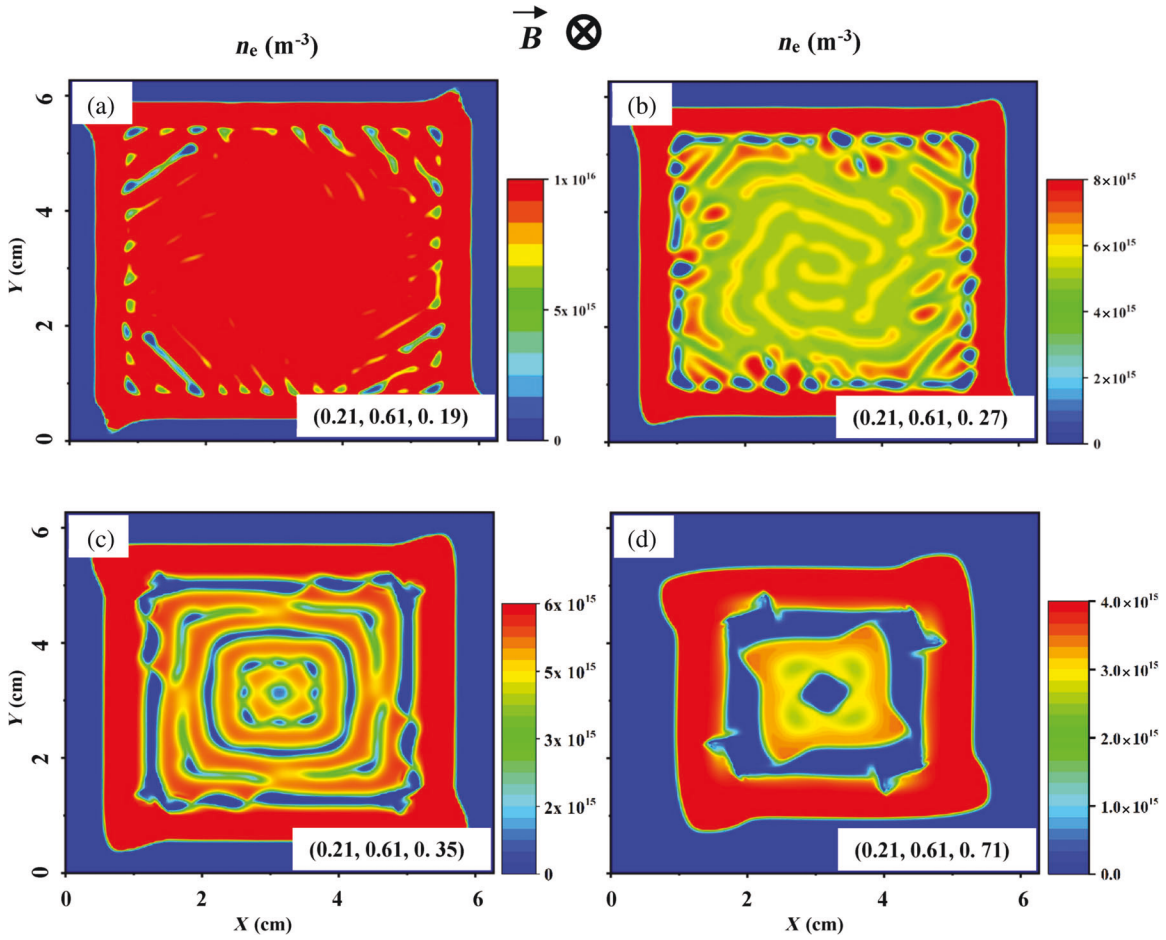

FIGURE 5 X-Y cross section of the electron density profile in magnetized argon plasma at different electron/ion densities. (a) 3.4×10^{15} m^{-3}, (b) 2.0×10^{15} m^{-3}, (c) 1.1×10^{15} m^{-3}, (d) 2.7×10^{14} m^{-3}. In all these cases, the neutral gas pressure is $P = 15$ Pa, the plasma is exposed to $B = 0.8$ T magnetic field, $T_e = 2.5$ eV and $T_i = 0.025$ eV. The set of three length parameters, (r_i (mm), λ_i (mm), λ_{De} (mm)), is also displayed on each graph. By increasing the electron/ion density so that the Debye length drops below the ion gyro-radius, no significant filamentary pattern forms in the magnetized plasma

Based upon the potential and density graphs presented in Figure 7, we assume the following functions for the periodic variation of electron/ion densities in the depletion regions with location along x-axis:

$$n_e = n_0 - n_{e1}\sin\left(\frac{\pi x}{w_d}\right) \qquad 0 \le x < w_d \tag{8}$$

$$n_i = n_0 - n_{i1}\sin\left(\frac{\pi x}{w_d}\right) \qquad 0 \le x < w_d \tag{9}$$

where n_e is the local electron density, n_i is the local ion density, n_0 is the initial background electron/ion density (mostly $n_0 = 5.4\times10^{14}$ m^{-3} in the presented simulations), n_{e1} is the amplitude of the electron density in the depletion regions relative to n_0, n_{i1} is the drop of the ion density in the depletion regions relative to n_0, and w_d is the width of the depletion region.

Based on the proposed stability mechanism, at the boundary of the filament and depletion region, the repulsive force from the excess of the ions in the depletion region cancels out the force due to gradient of ions density from the filament to the depletion region (also see Figure 7):

$$en_iE_x = K_bT_i\frac{\partial n_i}{\partial x} \qquad (\text{at } x = w_d) \tag{10}$$

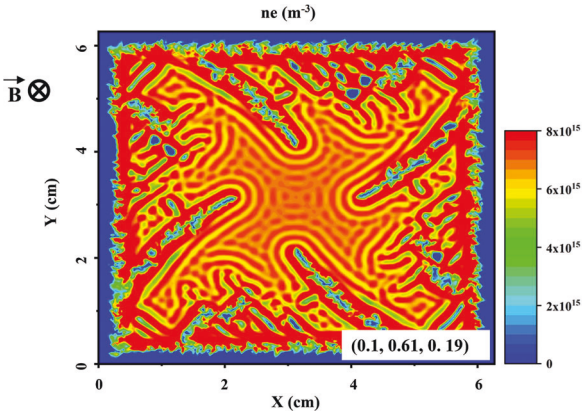

FIGURE 6 X-Y cross section of the electron density profile in argon plasma for $P = 15$ Pa and $n_e = n_i = 3.4 \times 10^{15}$ m^{-3}, $T_e = 2.5$ eV and $T_i = 0.025$ eV, exposed to 1.6 T magnetic field. The set of three length parameters, (r_i (mm), λ_i (mm), λ_{De} (mm)), is also displayed on the graph. This graph compared to Figure 45.a shows that when the ion gyro-radius is made smaller than the electron Debye length, the filaments can re-form in the plasma

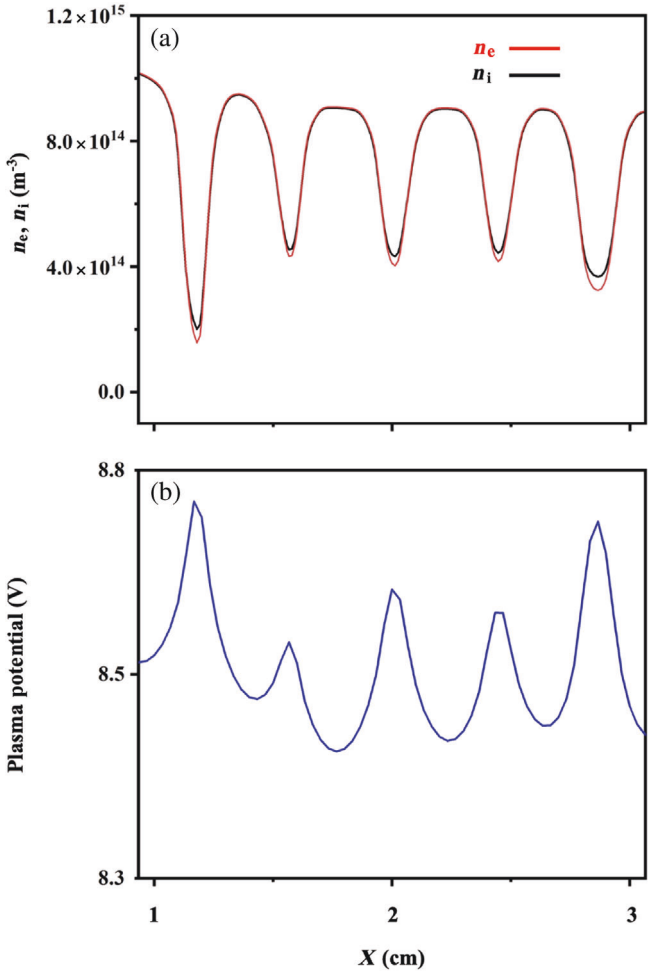

FIGURE 7 (a) Electron and ion densities along x-axis in the middle of the plasma chamber. (b) Plasma potential along x-axis in the middle of the plasma chamber. The electron/ion density as well as the plasma potential can be expressed as a sinusoidal function in the depletion regions where ne, ni and the plasma potential drop to their minimum values

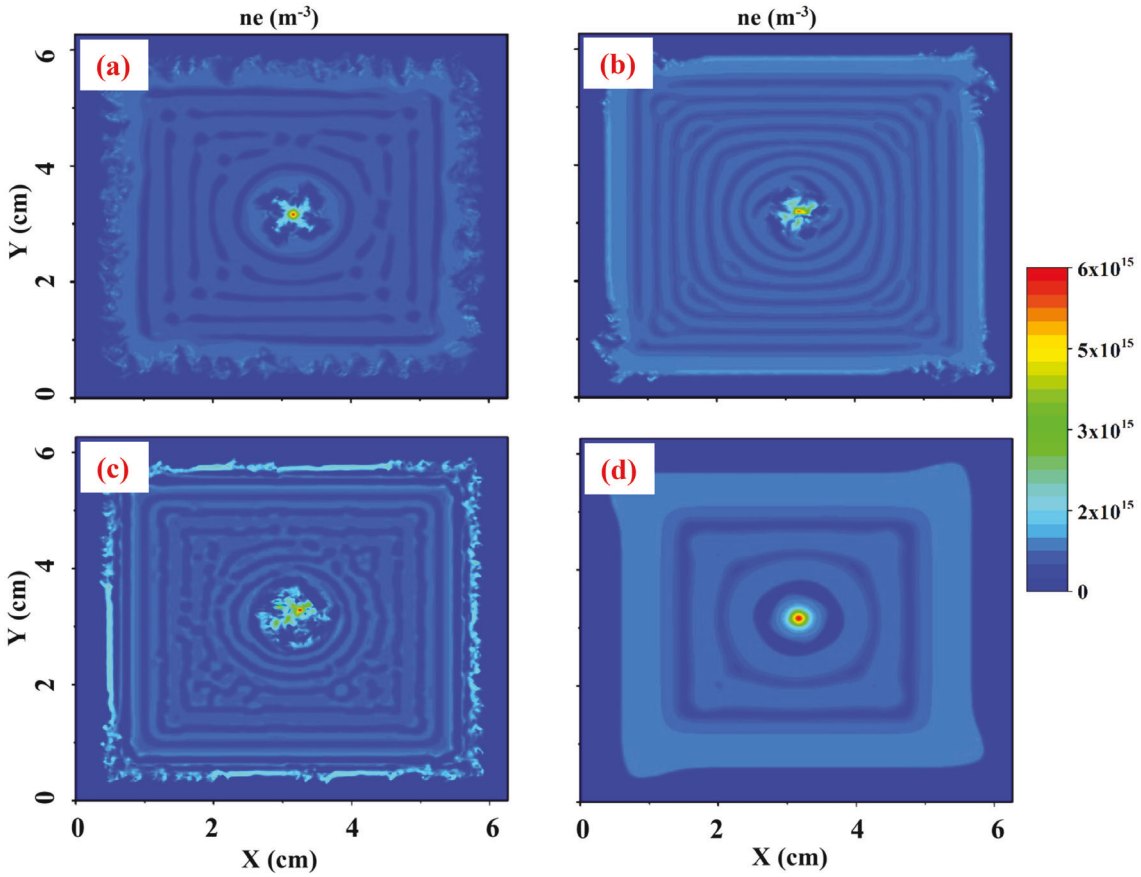

FIGURE 8 Top view of different filamentary patterns forming in a magnetized argon plasma due to different plasma parameters or geometry. The average width of the depletion regions, W_d, in these patterns are calculated using both Equation (12) and by measuring their average width in the graphs. The corresponding initial condition for each graph and the average widths are given in Table 1. Also, electron/ion temperature are assumed to be $T_e = 2.5$ eV and $T_i = 0.025$ eV respectively

where e is the unit charge, E_x is the X-component of the electric field vector, K_b is Boltzmann constant, and T_i is the ion temperature, which is assumed to be constant. Along with these equations, Poisson's equation in the middle of the plasma chamber can be written as follows:

$$\frac{\partial E_x}{\partial x} = \frac{e(n_i - n_e)}{\varepsilon_0} \tag{11}$$

where ε_0 is the electric permittivity of free space. Solving for w_d from Equations (8) to (11):

$$w_d^2 = \frac{\varepsilon_0 K_b T_i}{e^2 n_0} \frac{\pi^2 n_{i1}}{(n_{e1} - n_{i1})} \tag{12}$$

$$w_d^2 = \lambda_e^2 \frac{T_i}{T_e} \frac{\pi^2 n_{i1}}{(n_{e1} - n_{i1})} \tag{13}$$

where λ_e is the electron Debye length.

Although the rise and drop of electron/ion density (n_{e1}, n_{e2}, n_{i1}, and n_{i2}) are required to precisely predict the width of the filaments, Equation (13) confirms the effect of the electron Debye length (plasma density) on the characteristics of the filamentary structures, which had been previously observed in the experiments.[25,29] Equations (12) and (13) are also consistent with the observations presented in Figure 5 in which by increasing the Debye length (decreasing the plasma density) the filamentary curves get wider and further away from one another. The parameters n_{e1} and n_{i1} depend on different plasma parameters as well as the geometry of the plasma chamber and the applied magnetic field strength.

TABLE 1 The corresponding initial condition for each graph and the average widths

	(a)	(b)	(c)	(d)
Plasma density	5×10^{14} m^{-3}	1×10^{15} m^{-3}	5×10^{14} m^{-3}	5×10^{14} m^{-3}
Pressure	9 Pa	9 Pa	9 Pa	18 Pa
Magnetic field	1 T	1 T	1 T	0.8 T
Electrode gap	4.2 cm	4.2 cm	1.2 cm	4.2 cm
W_d from Equation (12)	1.9 mm	1.3 mm	1.3 mm	3.5 mm
W_d from the graph	1.8 mm	1.4 mm	1.5 mm	3.3 mm

To investigate the equation derived to relate the width of the depletion region in a patterned magnetized plasma to various plasma parameters (Equation 12), the width of the depletion regions is measured manually in the obtained simulation graphs and by using Equation (12). Figure 8 displays few different filamentary patterns appearing in the magnetized plasma due to different initial conditions or plasma chamber geometry. For each of these graphs, the average width of the filaments, W_d, is calculated using Equation (12) and by measuring their average width in the graphs. As it can be seen in this figure, these two measurements of the filament's width are in good agreement, which is another evidence of the validity of the proposed model for filamentary pattern formation in magnetized plasmas (Table 1).

4 | CONCLUSION

This paper has described numerical and theoretical investigation of magnetized plasma and dusty plasmas. Because of experimental challenges associated with the study of strongly magnetized plasmas, simulations provide an effective technique for studying the properties of these systems. Most importantly, in order to understand the dynamics and behaviour of the dust particles in magnetized dusty plasmas, it is crucial to precisely study the dynamics of the background plasma. The study of self-organized pattern formation in strongly magnetized plasma presented in this work is intended to serve that goal.

In this work, the correlation between the properties of the filamentary patterns in magnetized plasmas with characteristic length parameters of ion gyro-radius, ion-neutral mean-free-path, and electron Debye length was investigated. It was shown that for the self-organized patterns to form in the magnetized plasma the ion gyro-radius should be smaller than both ion-neutral mean-free-path and electron Debye length. This offers a possible explanation for the experimental observations of the dependency of filamentation phenomenon on neutral gas pressure due to its role in ion-neutral mean-free-path and the input power as a representation of plasma density and the electron Debye length.

Moreover, it was shown that there is a slight imbalance between electron and ion densities in the filaments and depletions regions, which generates an electric field structure that maintains the filamentary patterns. By analysing these results, a theoretical equation was derived that relates the width of the patterns and the electron Debye length. This equation was verified in multiple simulations of filamentation phenomenon.

Finally, this work contributes to the larger body of experimental and theoretical studies of dusty plasmas that have been pioneered by the research contributions of Prof. Fortov. His long legacy will continue to shape this work and the field of dusty plasmas into the future. We are pleased to honour his memory with this paper.

ACKNOWLEDGEMENT

This work was supported by funds from the National Science Foundation EPSCoR program (OIA-1655280) and US Department of Energy (SC-0016330).

DATA AVAILABILITY STATEMENT

The data that support the findings of this study are available from the corresponding author upon reasonable request.

REFERENCES

[1] H. Ikezi, *Phys. Fluids* **1986**, *29*, 1764.
[2] J. Chu, LI, *Phys. Rev. Lett.* **1994**, *72*, 4009.

[3] H. Thomas, G. Morfill, V. Demmel, J. Goree, B. Feuerbacher, D. Möhlmann, *Phys. Rev. Lett.* **1994**, *73*, 652.
[4] N. Rao, P. Shukla, M. Yu, *Planet. Space Sci.* **1990**, *38*, 543.
[5] A. Barkan, R. Merlino, N. D'Angelo, *Phys. Plasmas* **1995**, *2*, 3563.
[6] A. Piel, A. Homann, A. Melzer, *Plasma Phys. Control. Fusion* **1999**, *41*, A453.
[7] G. Morfill, A. Ivlev, J. Jokipii, *Phys. Rev. Lett.* **1999**, *83*, 971.
[8] V. E. Fortov, A. P. Nefedov, V. M. Torchinskii, V. I. Molotkov, et al., *J. Exp. Theor. Phys. Lett.* **1996**, *64*, 92.
[9] V. E. Fortov, A. P. Nefedov, V. M. Torchinsky, V. I. Molotkov, O. F. Petrov, A. A. Samarian, A. M. Lipaev, A. G. Khrapak, *Phys. Lett. A* **1997**, *229*, 317.
[10] V. E. Fortov, V. I. Molotkov, A. P. Nefedov, O. F. Petrov, *Phys. Plasmas* **1999**, *6*, 1759.
[11] V. Fortov, A. Nefedov, O. Vaulina, A. Lipaev, et al., *J. Exp. Theor. Phys.* **1998**, *87*, 1087.
[12] A. Nefedov, O. Vaulina, O. Petrov, V. Molotkov, et al., *J. Exp. Theor. Phys.* **2002**, *95*, 673.
[13] V. Fortov, O. Vaulina, O. Petrov, V. Molotkov, et al., *Phys. Rev. Lett.* **2003**, *90*, 245005.
[14] A. P. Nefedov, O. S. Vaulina, O. F. Petrov, V. I. Molotkov, et al., *N. J. Phys.* **2003**, *5*, 108.
[15] V. E. Fortov, A. P. Nefedov, V. D. Lakhno, *Phys. Lett. A* **1998**, *250*, 149.
[16] M. M. Vasil'ev, L. G. D'yachkov, S. N. Antipov, O. F. Petrov, V. E. Fortov, *JETP Lett.* **2007**, *86*, 358.
[17] L. G. D'yachkov, O. F. Petrov, V. E. Fortov, *Contrib. Plasma Phys.* **2009**, *49*, 134.
[18] M. M. Vasiliev, L. G. D'yachkov, S. N. Antipov, R. Huijink, O. F. Petrov, V. E. Fortov, *EPL* **2011**, *93*, 15001.
[19] E. Thomas Jr., R. L. Merlino, M. Rosenberg, *Plasma Phys. Control Fusion* **2012**, *54*, 124034.
[20] E. Thomas, U. Konopka, D. Artis, B. Lynch, S. LeBlanc, S. Adams, R. L. Merlino, M. Rosenberg, *J. Plasma Phys.* **2015**, *81*, 345810206.
[21] E. Thomas Jr., B. Lynch, U. Konopka, R. L. Merlino, M. Rosenberg, *Phys. Plasmas* **2015**, *22*, 030701.
[22] T. Hall, E. Thomas Jr., K. Avinash, R. Merlino, M. Rosenberg, *Phys. Plasmas* **2018**, *25*, 103702.
[23] M. Menati, T. Hall, B. Rasoolian, L. Couedel, E. Thomas Jr., U. Konopka, *Plasma Sources Sci. Technol.* **2020**, *29*, 085015.
[24] U. Konopka, M. Schwabe, C. Knapek, M. Kretschmer, G. E. Morfill, *AIP* **2005**, *799*, 181.
[25] M. Schwabe, U. Konopka, P. Bandyopadhyay, G. E. Morfill, *Phys. Rev. Lett.* **2011**, *106*, 215004.
[26] E. Thomas Jr., B. Lynch, U. Konopka, M. Menati, S. Williams, R. L. Merlino, M. Rosenberg, *Plasma Phys. Control. Fusion* **2019**, *62*, 014006.
[27] M. Menati, E. Thomas Jr., M. J. Kushner, *Phys. Plasmas* **2019**, *26*, 063515.
[28] E. Thomas, B. Lynch, U. Konopka, M. Menati, S. Williams, R. L. Merlino, M. Rosenberg, *Plasma Phys. Control. Fusion* **2020**, *62*, 014006.
[29] M. Menati, B. Rasoolian, E. Thomas Jr., U. Konopka, *Phys. Plasmas* **2020**, *27*, 022101.
[30] I. H. Hutchinson, *Plasma Phys. Control Fusion* **2002**, *44*, 2603.
[31] R. L. Merlino, *Am. J. Phys.* **2007**, *75*, 1078.
[32] F. F. Chen, *Introduction to Plasma Physics and Controlled Fusion*. in Introduction to Plasma Physics and Controlled Fusion, New York, Springer, **1984**.
[33] M. A. Lieberman, A. J. Lichtenberg, *Principles of Plasma Discharges and Materials Processing*. in Principles of Plasma Discharges and Materials Processing: Second Edition, Hoboken, John Wiley & Sons, Inc, **2005**.

How to cite this article: M. Menati, U. Konopka, E. Thomas, *Contributions to Plasma Physics* **2021**, *61*(10), e202100083. https://doi.org/10.1002/ctpp.202100083